TSH Signaling Overcomes B-RafV600E–Induced Senescence in Papillary Thyroid Carcinogenesis through Regulation of DUSP6[1,2]

Young Hwa Kim*,[†], Yong Won Choi*,[†], Jae Ho Han[‡], Jeonghun Lee[§], Euy Young Soh[§], So Hyun Park[‡], Jang-Hee Kim[‡] and Tae Jun Park*,[†]

*Department of Biochemistry and Molecular Biology, Ajou University School of Medicine, Suwon, South Korea; [†]Department of Biomedical Sciences, Graduate School, Ajou University, Suwon, South Korea; [‡]Department of Pathology, Ajou University School of Medicine, Suwon, South Korea; [§]Department of Surgery, Ajou University School of Medicine, Suwon, South Korea

Abstract

B-RafV600E oncogene mutation occurs most commonly in papillary thyroid carcinoma (PTC) and is associated with tumor initiation. However, a genetic modification by B-RafV600E in thyrocytes results in oncogene-induced senescence (OIS). In the present study, we explored the factors involved in the senescence overcome program in PTC. First of all, we observed down-regulation of p-extracellular signal-regulated kinases 1/2 and up-regulation of dual specific phosphatase 6 (DUSP6) in the PTC with B-RafV600E mutation. DUSP6 overexpression *in vitro* induced extracellular signal-regulated kinases 1/2 dephosphorylation and inhibited B-RafV600E–induced senescence in thyrocytes. Although DUSP6 protein was degraded by B-RafV600E–induced reactive oxygen species (ROS), thyroid-stimulating hormone (TSH) stabilized DUSP6 protein by increasing Mn superoxide dismutase expression and inhibited B-RafV600E–induced senescence. Although serum TSH was not increased, its receptor was markedly upregulated in PTC with B-RafV600E. Furthermore, TSH together with DUSP6 reactivated Ras signaling, resulted in activation of Ras/AKT/glycogen synthase kinase 3β, and stabilized c-Myc protein by inhibiting its degradation. These observations led us to conclude that increased TSH signaling overcomes OIS and is essential for B-RafV600E–induced papillary thyroid carcinogenesis.

Neoplasia (2014) 16, 1107–1120

Introduction

Thyroid tumors are the most common endocrine malignancy, and papillary thyroid carcinoma (PTC) accounts for more than 70% of all thyroid cancers [1]. PTCs are known to frequently harbor activating mutations in B-Raf kinase, among which the change of valine to glutamic acid at the residue 600 (B-RafV600E) is the most common in PTCs [2,3]. B-RafV600E has also been reported in other cancers such as melanoma and colorectal and ovarian cancers [4–7] and known to be involved in early stage of carcinogenesis [4,5,8]. However, B-RafV600E is also known to induce senescence-like

growth inhibitory responses when ectopically expressed in primary normal cells, including human dermal fibroblasts, melanocytes, and thyrocytes [9–11]. This phenomenon is called "oncogene-induced senescence" (OIS), first identified by Serrano et al. [12]. OIS is currently considered as a tumor-suppressive mechanism, which is triggered in the face of aberrant Raf/mitogen activated protein kinase kinase/Erk activation [13,14]. To overcome OIS and to undergo a malignant transformation, therefore, additional stimuli such as tumor suppressor gene inactivation, additional oncogene activation [15], and attenuation or inactivation of aberrant Raf/mitogen activated protein kinase kinase/Erk signaling are required [13,14]. Interestingly, previous studies revealed no change of extracellular signal-regulated kinases 1/2 (Erk1/2) phosphorylation in cancer tissues from patients with B-RafV600E PTC [16,17], because phosphorylation of Erk1/2 is regulated by a negative feedback mechanism [18,19] and dual specific phosphatases (DUSPs) are suggested to be associated with a low level of phosphorylated Erk1/2 [20]. Furthermore, among DUSPs, up-regulation of DUSP6 has been reported in PTC with B-RafV600E [16,21–23]. However, the role and regulation mechanism of DUSP6 in B-RafV600E–induced papillary thyroid carcinogenesis remain unclear.

In contrast to animal models of other cancers with B-RafV600E [24–26], thyrocyte-specific expression of B-RafV600E was known to be enough to induce PTC in transgenic mice [27,28]. However, animal studies suggested the importance of thyroid-stimulating hormone (TSH) signaling in B-RafV600E–induced thyroid carcinogenesis [27,29]. B-RafV600E could not induce any thyroid cancer if TSH is under normal range, and B-RafV600E is expressed in postnatal thyroid, which is a condition more similar to human sporadic PTCs [29]. However, it is unclear how TSH signaling facilitates B-RafV600E tumorigenesis.

In the present study, therefore, we first investigated the effect of B-RafV600E in normal isolated thyrocytes and compared the results with those of human tissues from patient with B-RafV600E–positive PTC. Furthermore, we analyzed the effect of TSH on B-RafV600E–induced OIS in primary thyrocytes to test a hypothesis that TSH signaling could abolish B-RafV600E–induced senescence. We found that B-RafV600E–induced OIS could be overcome by up-regulation of TSH signaling through the regulation of the DUSP6 activity.

Materials and Methods

Tumor Samples from Patients

Fresh tissues from PTC were obtained from patients at Ajou University Hospital after surgical resection with informed consent. Fresh tumor and normal tissues were separately sampled in the representative areas by an experienced pathologist and snap frozen in liquid nitrogen immediately after resection, according to the specimen regulation of Ajou University Hospital. Patients who had a past history of chemotherapy or radiation therapy before the surgery were excluded from the study.

Cloning of B-RafV600E, DUSP6, and c-Myc and Lentivirus Preparation

B-Raf wild-type, V600E mutant, c-Myc, and DUSP6 were cloned from normal thyroid and PTC in our laboratory. After insertion of cDNA into the TOPO cloning vector (Invitrogen, Carlsbad, CA) and sequencing, cDNAs were inserted into the pCDH-CMV-MCS-EF1-Puro lentivirus vector (System Biosciences, Mountain View, CA). To generate lentiviral particles, HEK-293TN cells were transfected with plasmid DNA (pGag-pol, pVSV-G, and pCDH-B-Raf or pCDH-B-RafV600E) [30].

Isolation and Culture of Thyrocytes

Normal and tumor thyrocytes were isolated from human tissues. Briefly, thyroid tissue was cut into small pieces and washed five times with phosphate-buffered saline (PBS). Enzymatic digestion was carried out by adding 0.2% collagenase I (Worthington Biochemical, Lakewood, NJ) in Hepes buffer (30 mM Hepes, 130 mM NaCl, 4 mM glucose, and 1 mM phosphate buffer), with gentle shaking for 6 hours at 32°C. The cells were centrifuged at 1500 rpm for 5 minutes and washed three times with PBS. The cell pellet was resuspended in complete media (F12K; Gibco BRL, Bethesda, MD; TSH, 10 mU/ml; insulin, 0.01 mU/ml; hydrocortisone, 10 nM; transferring, 0.005 mg/ml; somatostatin, 10 ng/ml; glycyl-L-histidyl-L-lysine acetate, 10 ng/ml; Sigma, St Louis, MO) and placed into 10-cm tissue culture dishes. Immunocytochemical analysis detected two kinds of thyrocyte-specific proteins including thyroglobulin and thyroid transcription factor 1 (data not shown). SNU790 PTC cell line was purchased from Korean Cell Line Bank (KCLB, Seoul, Korea).

Immunohistochemistry and Immunocytochemistry

Immunohistochemical staining was performed with primary antibodies on 4-μm-thick representative tissue sections of formalin-fixed paraffin-embedded tissue section in the Benchmark XT automated immunohistochemistry stainer (Ventana Medical Systems Inc, Tucson, AZ). The primary antibodies used were given as follows: total Erk1/2, 1:700 and p-Erk1/2, 1:400 (Cell Signaling Technology, Danvers, MA); B-RafV600E, 1:50 (Clone VE1; Spring Bioscience, Pleasant, CA); c-Myc, 1:400; c-Myc^{T58}, 1:75; TSH receptor (TSHR), 1:1500 (Abcam, Cambridge, MA); DUSP6, 1:1000 (Abnova, Walnut, CA); p16^{INK4A}, predilution (Roche, Tucson, AZ). Detection was done using the Ventana Optiview DAB Kit (Ventana Medical Systems).

Thyrocytes were cultured on a cover glass, fixed with 4% paraformaldehyde in PBS at 4°C for 20 minutes, and then washed three times with PBS containing 0.1% Tween 20. Cells were incubated with 1.5% horse serum in phosphate buffered saline containing 0.1% tween 20 for 1 hour at room temperature, and anti–p-Erk1/2 (Cell Signaling Technology), anti-TSHR (Abcam), or anti–γ-tubulin (Sigma) was then applied overnight at 4°C. The secondary antibody (1:500) was applied for 1 hour, and the cells were observed under fluorescence microscope (Axio Imager M1; Carl Zeiss, Oberkochen, Germany).

Analysis of B-RafV600E Mutation

We used three kinds of mutant analysis methods including restriction fragment length polymorphism (RFLP), direct sequencing, and immunohistochemistry. For genomic DNA isolation, one representative formalin-fixed paraffin-embedded tissue block of surgical specimens was selected and cut at 10-μm thickness. Genomic DNA was extracted from manually microdissected tumor area of each tissue section using a QIAamp DNA FFPE Tissue Kit (Qiagen, Hilden, Germany) according to the manufacturer's instruction. To detect B-RafV600E mutation, we initially performed polymerase chain reaction (PCR)–RFLP analysis [31]. The forward primer was 5′-TAAAAATAGGTGATTTTGGTCTAGCTCTAGCTCTAG-3′, and the reverse primer was 5′-ACTATGAAAATACTATAGTT-GAGA-3′. PCR was performed at 94°C for 30 seconds, 54°C for 30 seconds, and 72°C for 30 seconds for 35 cycles. After purification, the PCR products were digested with XbaI for 90 minutes, electrophoresed, and stained with ethidium bromide. The presence of B-

RafV600E mutation was ascertained when PCR-RFLP showed two bands. In case of negative or equivocal results for the B-RafV600E mutation with the RFLP method, we performed additional direct sequencing. Briefly, B-Raf exon 15 was amplified by PCR using the forward primer 5′-GCTTGCTCTGATAGGAAAATGAG-3′ and reverse primer 5′-GTAACTCAGCAGCATCTCAGG-3′. PCR was performed at 94°C for 30 seconds, 60°C for 30 seconds, and 72°C for 30 seconds for 34 cycles. After amplified products were purified, direct DNA sequencing was performed by Applied Biosystems 3500XL Genetic Analyzer with GeneMapper® Software v4.1 (Applied Biosystems, Foster City, CA). In addition to molecular analysis, we also performed immunohistochemical analysis using a mutation-specific monoclonal antibody, VE1, which was developed by Capper et al. [32].

Immunoprecipitation-Phosphatase Activity Assay

Immunoprecipitation (IP) with anti-DUSP6 IgG was performed with normal and B-RafV600E with or without TSH-treated thyrocyte lysate in a solution containing 20 mM Tris-HCl (pH 7.0), 1% Triton X-100, 0.25 M sucrose, 1 mM EDTA, 1 mM EGTA, 0.1% β-mercaptoethanol, 1 mM PMSF, and 1 μg/ml leupeptin by the standard method. DUSP6-IP-phosphatase assay mixture (200 μl) containing the above DUSP6 immunoprecipitates and 20 mM p-nitrophenyl phosphate in 50 mM succinate buffer was incubated at 37°C for 30 minutes, and the phosphate released was measured with an enzyme-linked immunosorbent assay reader (BioTek, Winooski, VT) at 405 nm.

Measurement of Ras Activity

GTP-bound Ras was incubated with Rho binding protein agarose conjugate (Millipore, Billerica, MA) for 30 minutes at 4°C in normal, B-RafV600E, B-RafV600E/DUSP6, SNU790, and SNU790/shDUSP6 cell lysates with or without TSH treatment for 5, 15, and 30 minutes. The bead was washed twice with washing buffer and dissolved in 2× sodium dodecyl sulfate (SDS) sample buffer, and then SDS–polyacrylamide gel electrophoresis was carried out. GTP-Ras was detected with anti-Ras (Millipore) antibody. Positive and negative controls were treated with 10 mM GTPγS or 100 mM guanosine diphosphate for 30 minutes, respectively.

Real-Time PCR Analysis

Total cellular RNAs were isolated from normal and PTC tissues. First-strand cDNA was synthesized by reverse transcription reaction using oligo-dT primers from 1 μg of total cellular RNA. Real-time PCR was carried out with Power SYBR Green PCR Master Mix (Applied Biosystems) using the following conditions: initial activation at 95°C for 5 minutes, followed by 40 cycles of 95°C for 15 seconds and 60°C for 1 minute. The primers used for real-time PCR were given as follows: Mn superoxide dismutase (SOD): 5′-GACCTGCCCTACGACTACG-3′, 5′-TGACCACCACCATT-GAACTT-3′; glutathione peroxidase-1 (GPx1): 5′-TTCCCGTG CAACCAGTTTG-3′, 5′-TTCACCTCGCACTTCTCGAA-3′; Cu/Zn SOD: 5′-AGGGCATCATCAATTTCGAG-3′, 5′-TGCCTCTCTTCATCCTTTGG-3′; catalase: 5′-TTTCCCAG GAAGATCCTGAC-3′, 5′-ACCTTGGTGAGATCGAATGG-3′; thiol-specific antioxidant: 5′-CCAGACGCTTGTCTGAGGAT-3′, 5′-ACGTTGGGCTTAATCGTGTC-3′; DUSP6: 5′-GAGTCT-GACCTTGACCGAGACCCC-3′, 5′-TTCCTCCAACACGTC CAAGTTGGT-3′; Ets1: 5′-CTGCGCCCTGGGTAAAGA-3′, 5′-CCCATAAGATGTCCCCAACAA-3′; c-Myc: 5′-GCCACGTCTC

CACACATCAG-3′, 5′-TGGTGCATTTTCGGTTGTTG-3′; p16^{INK4A}: 5′-CTGCCCAACGCACCGAATAG-3′, 5′-TACCGTGC GACATCGCGATG-3′; TSHR: 5′-CCCAGCTTACCGCCCAGT-3′, 5′-TAGAAAATGCATGACTTGGAATAGTTC-3′; β-actin: 5′-CCCTGGCACCCAGCAC-3′, 5′-GCCGATCCACACGGAGTAC-3′, respectively.

Measurement of Reactive Oxygen Species

Intracellular reactive oxygen species (ROS) was measured by using oxidation-sensitive fluorescent probe dichlorodihydrofluorescein diacetate (DCF-DA). Thus, thyrocytes or SNU790 cells were treated with DCF-DA (20 μM) for 10 minutes, and the cells were collected and washed with PBS. They were then transferred to 5-ml polystyrene round bottom tubes and subjected to flow cytometry (BD FASCanto II; BD Biosciences, San Jose, CA) for acquisition and analysis.

RNA Interference

For knockdown of DUSP6, TSHR, and B-Raf expression, shRNA was prepared in a pLKO lentiviral vector (Sigma) and then amplified in 293TN cells. Thyrocytes were plated and grown in 60-mm culture dishes. After overnight culture, they were infected with either target shRNA or a nonsilencing control shRNA. After infection of the lentivirus, the cells were selected for 1 to 2 weeks at a concentration of 3.5 μg/ml puromycin. shRNA sequences were given as follows: shB-Raf: 5′-TTACCTGGCTCACTAACTAAC-3′; shTSHR: 5′-GTTAGGCTACCAGCATATTTG-3′; shDUSP6: 5′-TCTAATC-CAAAGGGTATATTT-3′, respectively.

Senescence-Associated β-Galactosidase Staining

The cells or frozen tissue slides were fixed with 10% formalin for 10 minutes and then incubated with SA-β-gal solution (X-gal, 1 mg/ml; 40 mM citric acid/sodium phosphate, pH 6.0; 5 mM potassium ferrocyanide; 5 mM potassium ferricyanide; 150 mM NaCl; 2 mM MgCl$_2$) for 10 hours at 37°C. After washing with PBS, SA-β-gal–positive cells were then analyzed under light microscopy.

Analysis of DUSP6 Protein Stability

To evaluate the stability of the DUSP6 protein, control or B-RafV600E–expressing thyrocytes were treated with cycloheximide (25 μg/ml) at indicated times. The cell lysates were prepared and analyzed by Western blot analysis after separation on SDS–polyacrylamide gel electrophoresis. The band intensity was analyzed by a densitometer and represented as a score.

Statistical Analysis

Numerical data are presented as mean $\pm$ SD of independent determinations. Statistical analysis of differences was performed by Student's t test, and a P value <0.05 was considered as significant.

Results

B-RafV600E Induces OIS in Primary Thyrocytes

We generated lentivirus harboring B-RafV600E to express the mutant protein in isolated primary thyrocytes and found cellular enlargement and elongation with cytoplasmic vacuoles in the cells. These morphologic findings were consistent with cellular senescence but not transformation (Figure 1A). Furthermore, the results of growth analysis, SA-β-gal staining, and p16^{INK4A} mRNA analysis were compatible with cellular senescence in B-RafV600E–expressing thyrocytes (Figure 1B). Western blot analysis revealed that B-
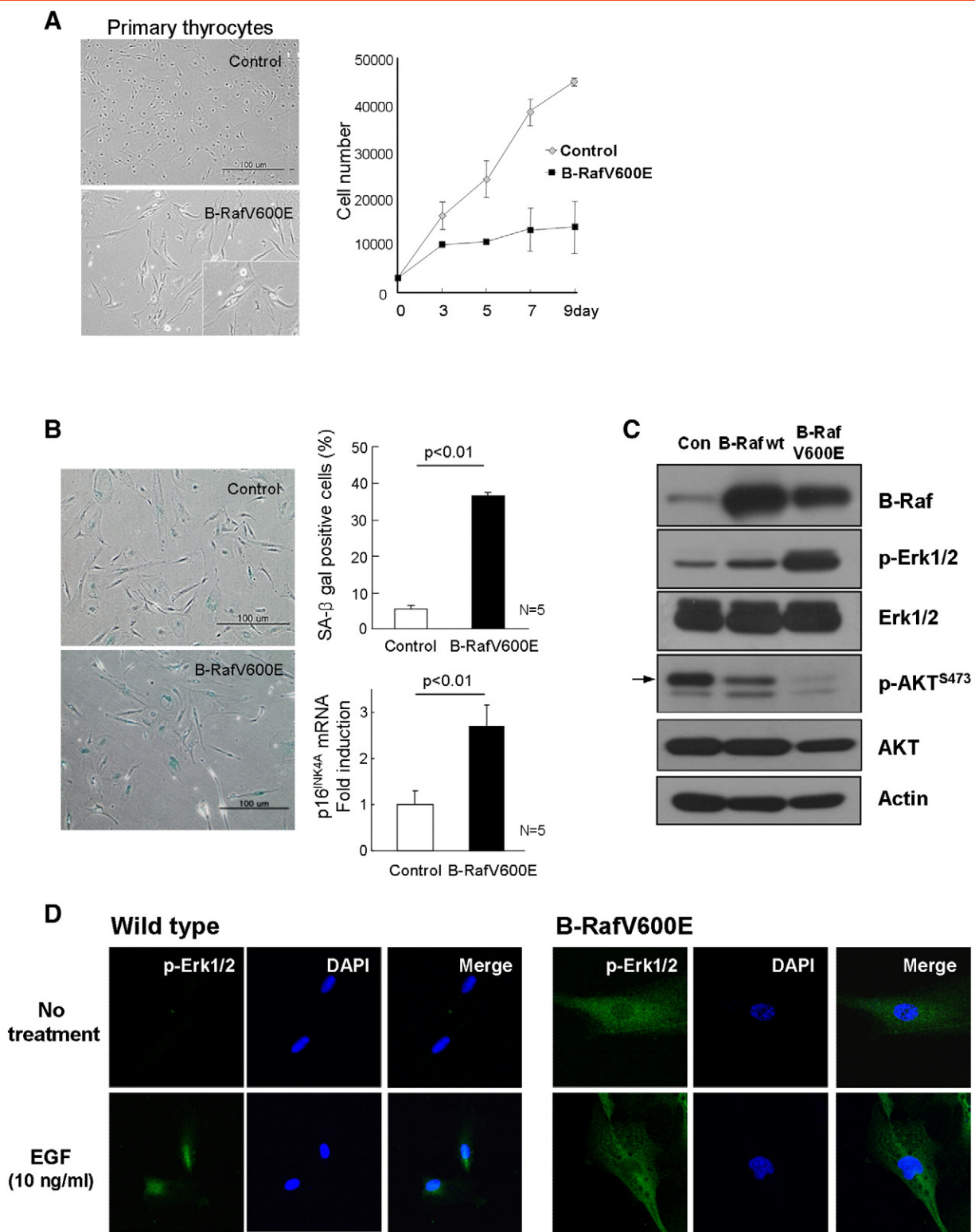
Figure 1. B-RafV600E induces OIS in isolated normal thyrocytes. (A) B-RafV600E–induced OIS in isolated normal thyrocytes. Normal thyrocytes were infected with control or B-RafV600E lentivirus and selected with puromycin for 1 week. The inset represents higher magnification field. (B) Expression of SA-β-gal and p16^INK4A was higher in B-RafV600E–expressing cells than in control. (C) Western blot analysis of B-Raf, p-Erk1/2, and AKT. Normal thyrocytes were infected with control, B-Raf wild-type, or B-RafV600E lentivirus, selected with puromycin for 1 week and then subjected to Western blot analysis. (D) Immunocytochemical analysis of p-Erk1/2 in normal and B-RafV600E–expressing thyrocytes. After epidermal growth factor treatment, translocation of p-Erk1/2 was analyzed in control or B-RafV600E lentivirus–infected thyrocytes, respectively.
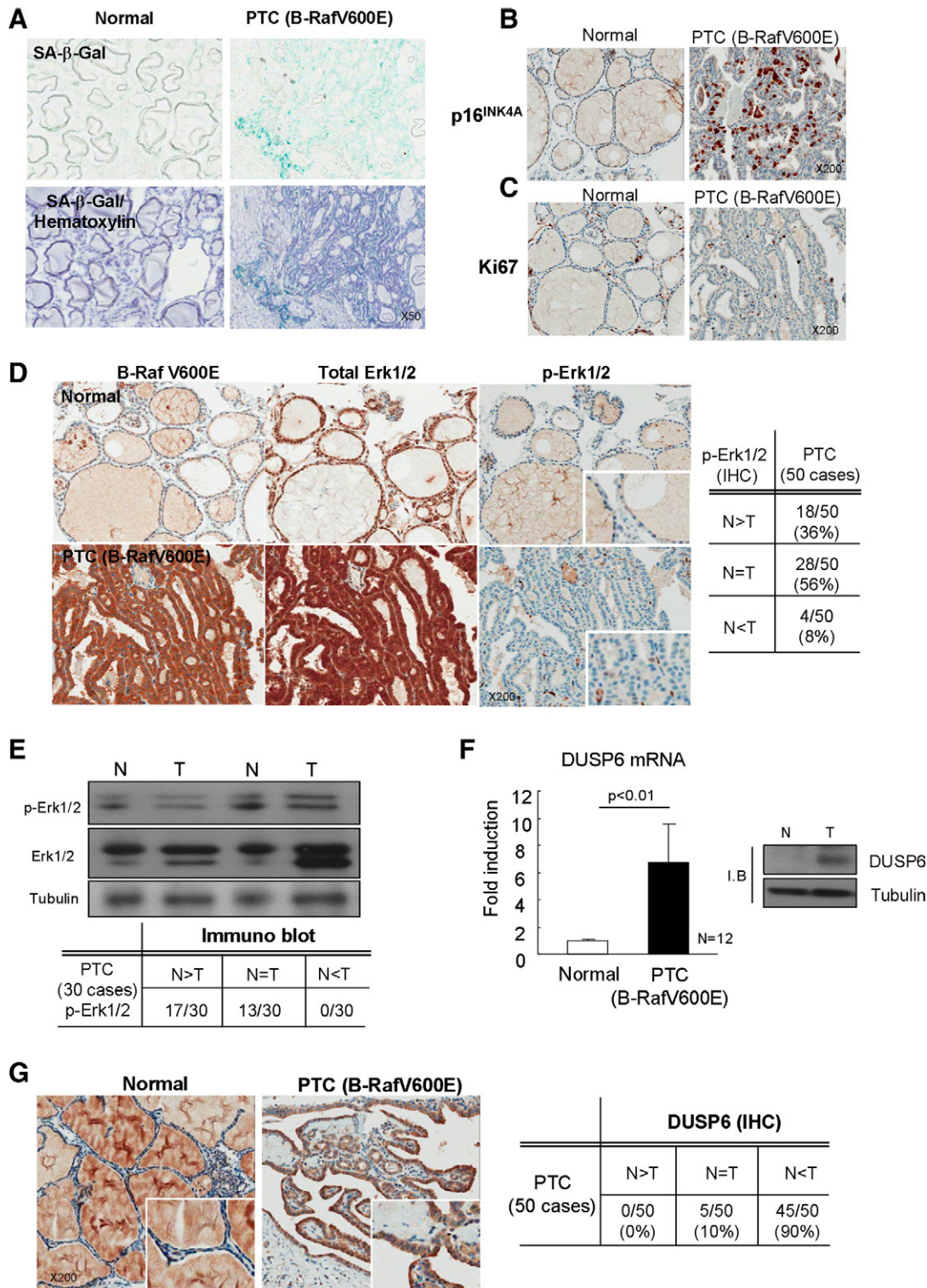
Figure 2. Cancer cells in B-RafV600E PTC tissues escape from senescence. (A) SA-β-gal–positive cancer cells were observed in B-RafV600E–harboring PTC tissue. Upper and lower panels show SA-β-gal and SA-β-gal/hematoxylin staining, respectively. (B) p16INK4A expression in B-RafV600E–harboring PTC tissues. (C) Ki67 expression in B-RafV600E–harboring PTC tissues. Phosphorylated Erk1/2 expression was analyzed by immunohistochemistry (D) and Western blot analysis (E). Normal and B-RafV600E PTC regions were serially sectioned and stained with B-RafV600E, Erk1/2, and p-Erk1/2, respectively. Fifty or 30 cases each of B-RafV600E PTC were analyzed with immunohistochemistry and Western blot analysis, respectively, and the expression level of p-Erk1/2 is presented as a table. (F) DUSP6 expression in PTC tissue was analyzed by real-time PCR and Western blot analysis. Twelve and 30 cases each of normal and B-RafV600E–harboring PTC regions were analyzed for DUSP6 mRNA and protein, respectively. Representative Western blot data are shown in this figure, and total cases of DUSP6 protein expression pattern are presented as a table in Figure 5. (G) Up-regulation of DUSP6 in RafV600E–harboring PTC tissues. Fifty cases of B-RafV600E PTC were analyzed for DUSP6 expression by immunohistochemistry, and the expression pattern of DUSP6 is presented as a table. The inset represents higher magnification field. N and T indicate normal and cancer, respectively.

A DUSP6 mRNA

B

C

D DUSP6 mRNA (B-RafV600E)   DUSP6 mRNA (B-RafV600E)

E

F Normal thyrocytes

B-RafV600E thyrocytes

G Catalase   TSA   Cu/ZnSOD   GPx1   MnSOD
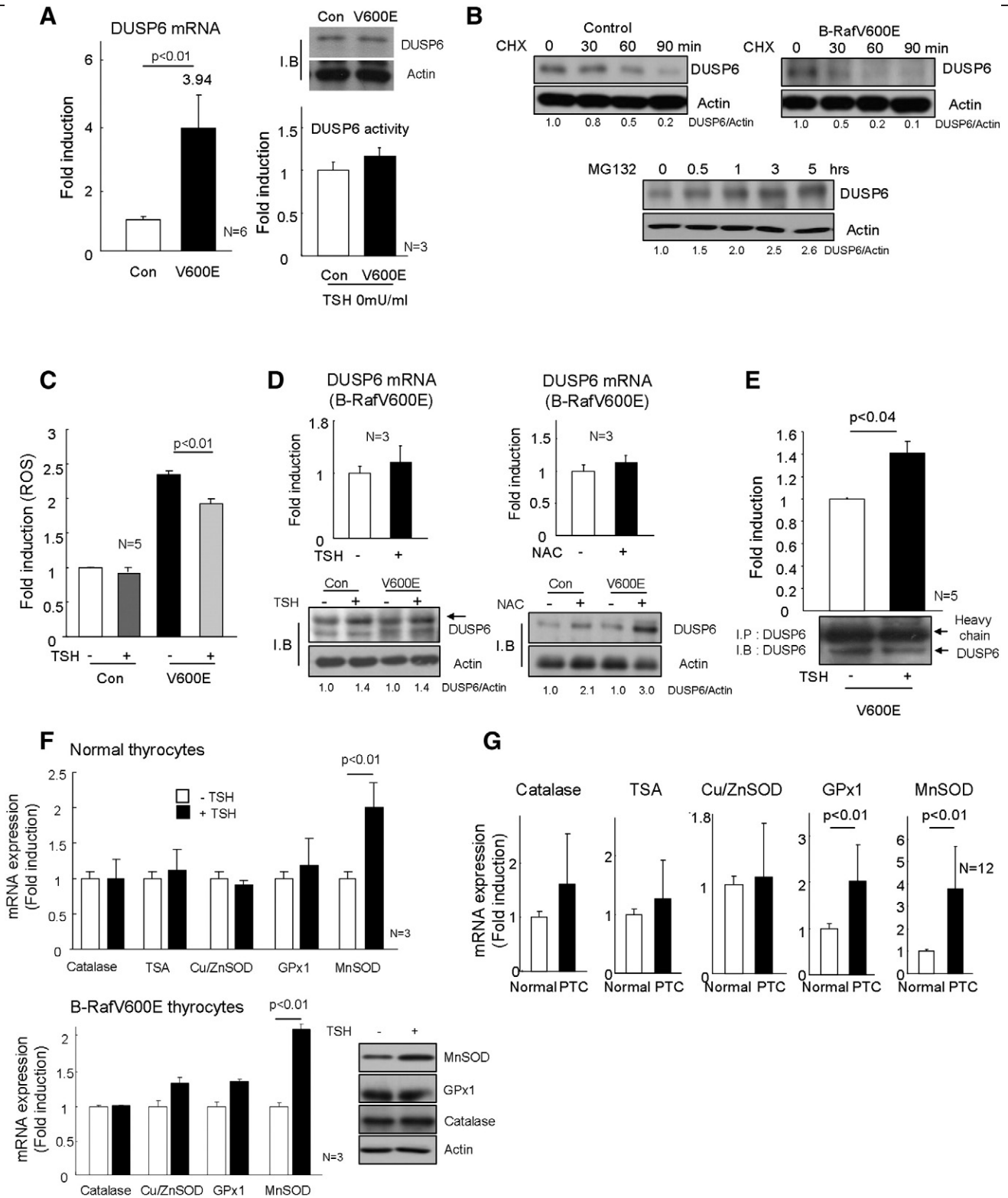
RafV600E induced Erk1/2 phosphorylation (Figure 1C). We further examined epidermal growth factor–induced phosphorylation and translocation of Erk1/2 and found that Erk1/2 was translocated into the nucleus only in normal thyrocytes, but not in B-RafV600E–transduced thyrocytes (Figure 1D). These data clearly indicated that B-RafV600E induced OIS in primary normal thyrocytes.

Cancer Cells in B-RafV600E PTC Tissues Escape from OIS

Next, we analyzed the role of B-RafV600E mutation in PTC tissues. Senescence has been found in the pre-malignant stage of tumor but not in malignant tumor [15,33,34]. However, we found that some of the cancer cells in B-RafV600E PTC tissues revealed SA-β-gal and p16^INK4A immunopositivity (Figure 2, A and B),

whereas some remaining cancer cells showed proliferation activity (Figure 2C). These findings suggested that senescence program was in progress in papillary thyroid carcinogenesis, and senescence as well as the cells that escaped from senescence co-existed in B-RafV600E PTC tissue. Furthermore, we observed that Erk1/2 phosphorylation was not increased in most of B-RafV600E PTCs (46/50 cases; 92%), despite the fact that B-RafV600E protein was highly expressed (Figure 2, D and E). Low level of Erk1/2 phosphorylation in PTC patient tissues has already been reported [16,17,23]. Thus, these data are consistent with previous publications data. This finding reflects that dephosphorylation of p-Erk1/2 actively occurred by phosphatase in B-RafV600E–harboring PTC [16,18–20]. Since previous studies reported increased expression of DUSP6 in PTC [16,21–23], we examined DUSP6 expression in B-RafV600E PTC tissues and found an up-regulation of DUSP6 (Figure 2, F and G). Moreover, as shown in the right panel of Figure S1, Erk1/2 phosphorylation was markedly downregulated in B-RafV600E–expressing cells when DUSP6 was lentivirally transferred. These data indicated that, in B-RafV600E PTC tissues, Erk1/2 phosphorylation could not be maintained due to DUSP6. Therefore, we next investigated the mechanisms involved in the dephosphorylation of p-Erk1/2 by DUSP6 in both B-RafV600E–harboring PTC tissues and isolated B-RafV600E–transduced thyrocytes.

TSH Increases DUSP6 Expression through Regulation of ROS Generation

Erk1/2 phosphorylation and DUSP6 expression are reciprocally regulated; DUSP6 expression is controlled by Erk1/2-Ets1 signaling, and expressed DUSP6 dephosphorylates p-Erk1/2 by feedback mechanism [18,19]. Indeed, Figure S2 shows up-regulation of Ets1 transcription factor in B-RafV600E PTC. Although DUSP6 mRNA expression in B-RafV600E–transduced thyrocytes was higher than normal cells, its protein expression and phosphatase activity were almost similar to those of normal thyrocytes (Figure 3A). In support of a recent study that DUSP6 was rapidly degraded in proteasome [35], we found that DUSP6 protein was rapidly degraded in B-RafV600E–transduced thyrocytes and stabilized by MG132 proteasomal inhibitor (Figure 3B). To exclude the possibility of DUSP6 degradation by autophagy, thyrocytes were treated with 3-methyladenine or E64d/pepstatin A; however, DUSP6 protein was not accumulated by autophagy inhibitors (Figure S3). In addition, we analyzed ROS generation because DUSP6 has been shown to be inactivated and degraded by ROS [35,36] and found marked up-regulation of ROS generation in B-RafV600E–transduced thyrocytes (Figure 3C). These data provided evidence that DUSP6 is likely inactivated, despite the fact that the level of DUSP6 mRNA was elevated in B-RafV600E–transduced thyrocytes and that reactivation or stabilization of DUSP6 are required to induce low level of p-Erk1/2 in PTC. Next, the effect of TSH on DUSP6 was investigated in B-RafV600E–expressing thyrocytes, since the dependency of B-Raf carcinogenesis of thyroid on TSH signaling has been demonstrated in genetically engineered mouse models [29]. Although TSH itself could not increase DUSP6 mRNA expression, slight increases in protein expression and the activity of phosphatase were observed in TSH-treated thyrocytes (Figure 3, D, left, and E). Next, we investigated ROS generation under the influence of TSH and found a decrease in ROS generation in B-RafV600E–expressing thyrocytes by TSH stimulation (Figures 3C and S4). To further confirm the ROS effect on DUSP6 expression, we employed N-acetylcysteine (NAC) to scavenge ROS and found that DUSP6 protein expression was increased by NAC without up-regulation of DUSP6 mRNA (Figure 3D, right panel). Since ROS generation was downregulated for 72 hours after TSH treatment (Figure S4), and TSH increased DUSP6 activity through regulation of ROS, we examined the expression of ROS scavenger proteins, such as catalase, Mn SOD, Cu/Zn SOD, GPx1, and thiol-specific antioxidant, and found that TSH increased Mn SOD expression (Figure 3F). We further analyzed antioxidant proteins mRNA expression in PTC by real-time PCR and found up-regulation of GPx1 and Mn SOD (Figure 3G). These data indicated that DUSP6 could be reactivated by TSH through the regulation of ROS generation.

TSH Signaling Inhibits B-RafV600E–Induced Senescence through DUSP6

Next, we evaluated the effect of DUSP6 on B-RafV600E–induced senescence using B-RafV600E/DUSP6 co-transduced thyrocytes. Figure 4, A and B, show significant reduction in the expression of SA-β-gal and p16^{INK4A} in B-RafV600E/DUSP6 co-transduced thyrocytes, indicating that DUSP6 overexpression inhibited OIS in the thyrocytes. These data led us to the hypothesis that reactivated DUSP6 by TSH could inhibit B-RafV600E–induced OIS. To verify this, we examined normal and B-RafV600E–transduced thyrocytes after TSH treatment. As expected, TSH treatment increased proliferation of normal and B-RafV600E–transduced thyrocytes

Figure 3. TSH increased DUSP6 activity. (A) B-RafV600E increased DUSP6 mRNA expression (left panel) but not protein expression and activity (right panel). Thyrocytes were infected with control or B-RafV600E lentivirus for 1 week, and then DUSP6 activity was analyzed by IP-phosphatase assay. Bar graph represents more than three independent experiments. (B) DUSP6 was degraded rapidly in B-RafV600E–expressing thyrocytes. Thyrocytes were treated with cycloheximide (CHX, 25 μg/ml) to inhibit translation at indicated times and analyzed for DUSP6 protein expression (upper panel). Thyrocytes were treated with MG132 (10 μM) at indicated times and DUSP6 stabilization was analyzed by Western blot analysis (lower panel). Number represents average of three independent experiments and indicates DUSP6/actin ratio compared with untreated data. (C) TSH inhibited ROS generation in B-RafV600E–expressing cells. Normal and B-RafV600E cells were treated with or without TSH (1 mU/ml) for 72 hours, and ROS generation was measured by FACS analysis. Bar graph represents five independent experiments. (D) DUSP6 expression in TSH-treated (1 mU/ml, 72 hours) thyrocytes (left panel). DUSP6 expression was measured by real-time PCR and Western blot analysis. Number indicates the ratio of DUSP6 to actin. The arrow indicates DUSP6. DUSP6 expression in NAC-treated (5 mM, 24 hours) thyrocytes (right panel). Number indicates the ratio of DUSP6 to actin. (E) TSH reactivated DUSP6 activity. DUSP6 activity was measured in B-RafV600E–expressing cells with or without TSH (1 mU/ml) treatment for 72 hours. Lower immunoblot figure shows immunoprecipitated DUSP6. (F) TSH induced Mn SOD expression. The expression of ROS scavenger proteins was analyzed by real-time PCR and Western blot with or without TSH (1 mU/ml, 24 hours) treatment in normal thyrocytes (upper panel) and B-RafV600E–expressing thyrocytes (lower panel), respectively. (G) Mn SOD expression was upregulated in PTC tissues. Twelve each of B-RafV600E mutant PTC and normal tissues were analyzed for mRNA of ROS scavenger proteins by real-time PCR.
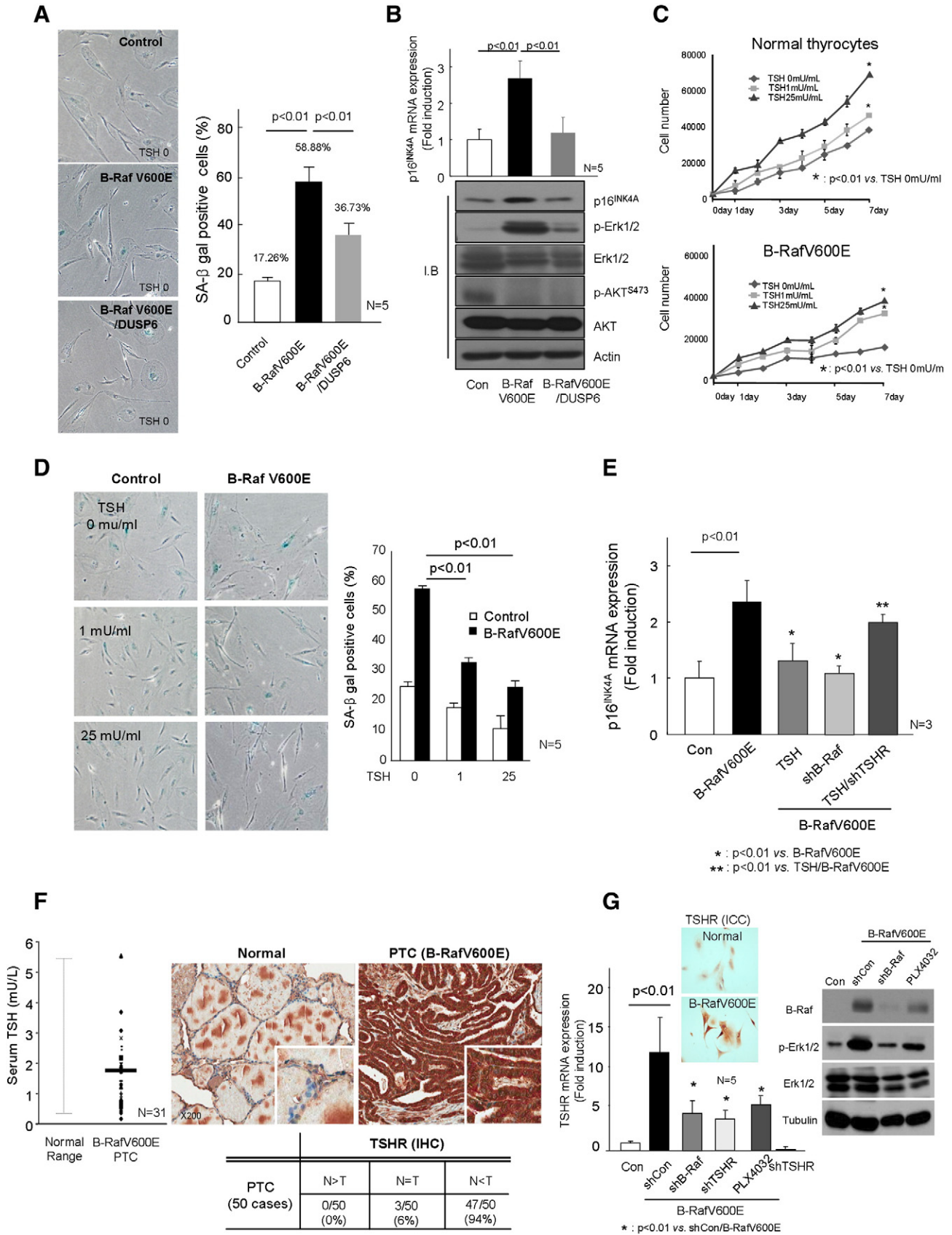
(Figure 4C) and also inhibited OIS induced by B-RafV600E (Figure 4, D and E), consistent with the result in Figure 3; TSH decreased ROS generation by regulation of Mn SOD expression and increased DUSP6 activity.

We then investigated the status of TSH in patients with B-RafV600E PTC, since we observed above that upregulated TSH signaling was an important factor to overcome B-RafV600E–induced senescence in thyroid carcinogenesis. However, no patients with B-RafV600E PTC showed a significant elevation of serum TSH (serum TSH range of patients: 0.19–5.56, average: 1.85, normal range: 0.35–5.5 mU/l; Figure 4F, left panel). We next examined the expression of TSHR in B-RafV600E–harboring PTC tissues and found diffuse strong immunoreactivity for TSHR in the cytoplasm as well as in the membrane of cancer cells, whereas there is only focal membranous staining in normal follicles (Figure 4F, right panel). To exclude the possibility of nonspecific antibody reaction, we analyzed TSHR mRNA expression in B-RafV600E PTC and found a moderate increase in TSHR mRNA expression (0.64- to 2.98-fold, 1.71 $\pm$ 0.74, $n = 23$, $P < .01$; Figure S5). We further accessed the effect of B-RafV600E on TSHR expression using cultured primary thyrocyte model. Real-time PCR and immunocytochemical analyses revealed that B-RafV600E increased the expression of TSHR in thyrocytes (Figure 4G). These data suggested that TSH signaling by its receptor overexpression could inhibit OIS in B-RafV600E PTC. Although TSH inhibited OIS in thyrocytes, the cells were not transformed *in vitro*. Therefore, our data raise the possibility of additional mechanism involved in papillary thyroid carcinogenesis.

Ras/AKT/c-Myc Signaling Is Reactivated by TSH and DUSP6

Inhibition of Ras activity by p-Erk1/2 is a well-characterized feedback signaling [37]. Phosphorylated Erk1/2 by B-RafV600E inhibited Ras-dependent AKT activation (Figure 5A, left pathway). However, in the presence of active DUSP6, p-Erk1/2 was unable to inhibit Ras any more, and Ras/AKT signaling was reactivated by ligand-receptor signaling (Figure 5A, right pathway). Indeed, reactivation of Ras (Figure 5B) and AKT phosphorylation were induced by TSH treatment in the presence of DUSP6 (Figure 5C). We further confirmed the feedback inhibition loop by inhibition of B-Raf. AKT phosphorylation was increased by a B-Raf inhibitor in B-RafV600E–expressing thyrocytes (Figure S6). Furthermore, when cancer cells from the B-RafV600E–harboring PTC were used, AKT signaling was activated by TSH (Figure 5D).

AKT signaling can activate several oncoproteins including c-Myc [38]. To test whether c-Myc could be activated by AKT signaling, we examined c-Myc expression in B-RafV600E PTC. However, c-Myc mRNA expression was found to be almost similar to that in normal thyroid region. Nevertheless, immunohistochemical staining and Western blot data showed higher protein expression of c-Myc in B-RafV600E PTC (Figure 5E), suggesting that up-regulation of c-Myc protein could be associated with a posttranslational event but not transcription. Therefore, the stability of c-Myc protein was evaluated by determining phosphorylation status on its Thr58 residue, since it is induced by GSK3β and phosphorylation on Thr58 residue of c-Myc increases its degradation by ubiquitination [39]. Figure 5F shows that TSH slightly decreased c-Myc^{T58} phosphorylation in B-RafV600E/DUSP6 but not in B-RafV600E only expressing cells. When c-Myc protein level was measured in cells treated with TSH for 24 hours, marked up-regulation of c-Myc was found in B-RafV600E/DUSP6 expressing thyrocytes (Figure 5F, lower panel). *In vivo* PTC tissue data clearly showed stabilization of c-Myc protein (Figure 5, G and H). These data suggested that Ras/AKT signaling reactivated by DUSP6 and TSH induced c-Myc stabilization and that stabilized c-Myc might be involved in thyroid carcinogenesis.

We further confirmed the effect of TSH signaling using B-RafV600E PTC cell lines (SNU790). Surprisingly, knockdown of TSHR induced down-regulation of cell proliferation (20% decrease, data not shown) along with an increase in ROS generation (Figure 6A) and a decrease in DUSP6 expression in the presence of TSH (Figure 6B). Furthermore, inhibition of DUSP6 by shRNA increased p-Erk1/2 expression and inhibited TSH-induced Ras activation (Figure 6, C and D). These data suggested that TSHR signaling is also important in maintaining malignant phenotype in established B-RafV600E cancer cell line.

Discussion

It is well established that OIS induction occurs when the oncogene is overexpressed [40,41]. In the present study, we evaluated the effects of B-RafV600E proteins, which are driven by a cytomegalovirus (CMV) promoter in the isolated thyrocytes by comparing with that of normal endogenous promoter in the B-RafV600E PTC. We found senescence program undergoing in both thyrocytes and PTC. Furthermore, some of thyrocytes in PTC tissue harboring B-RafV600E were found to undergo senescence program, whereas others escaped, strongly suggesting that senescence escape program

Figure 4. TSH signaling inhibits B-RafV600E–induced senescence. (A) DUSP6 inhibited B-RafV600E–induced OIS. Control or B-RafV600E lentivirus was co-infected with or without DUSP6 lentivirus and selected with 3.5 μg/ml puromycin for 2 weeks. Senescence cells were analyzed with SA-β-gal staining. p16^{INK4A} expression was analyzed in B-RafV600E and DUSP6 co-infected cells by real-time PCR (upper panel) and Western blot analysis (lower panel) (B). All of the bar graphs represent five independent experiments. (C) TSH accelerated cell proliferation in normal and B-RafV600E mutant expressing thyrocytes. Thyrocytes were infected with control or B-RafV600E lentivirus and selected with puromycin for 1 week; 3×10^3 cells were seeded with or without TSH, and the cell number was counted at indicated times. (D) TSH inhibited B-RafV600E–induced OIS. Normal thyrocytes were infected with control or B-RafV600E lentivirus and selected with 3.5 μg/ml puromycin for 2 weeks with or without TSH, and senescence cells were then analyzed with SA-β-gal staining. (E) p16^{INK4A} expression in B-RafV600E–expressing cells with or without TSH (1 mU/ml) was analyzed by real-time PCR. (F) TSH and TSHR expression in PTC patients. Serum TSH level was analyzed in 31 B-RafV600E–harboring PTC patients (left panel). Marked elevation of TSHR expression in B-RafV600E–harboring PTC (right panel). The inset shows higher magnification field. TSHR expression was analyzed by immunohistochemistry in 50 cases of B-Raf mutant–type PTC, and the expression level is presented (table). (G) B-RafV600E induced up-regulation of TSHR mRNA in thyrocytes. TSHR expression was analyzed by real-time PCR and immunocytochemistry. Thyrocytes were infected with control, B-RafV600E, B-RafV600E/shB-Raf, or B-RafV600E/shTSHR for 1 week and then analyzed for TSHR expression by real-time PCR. In the case of the B-Raf inhibitor study, B-RafV600E–infected thyrocytes were treated with PLX4032 (20 μM) for 24 hours and then analyzed. N and T indicate normal and cancer, respectively.
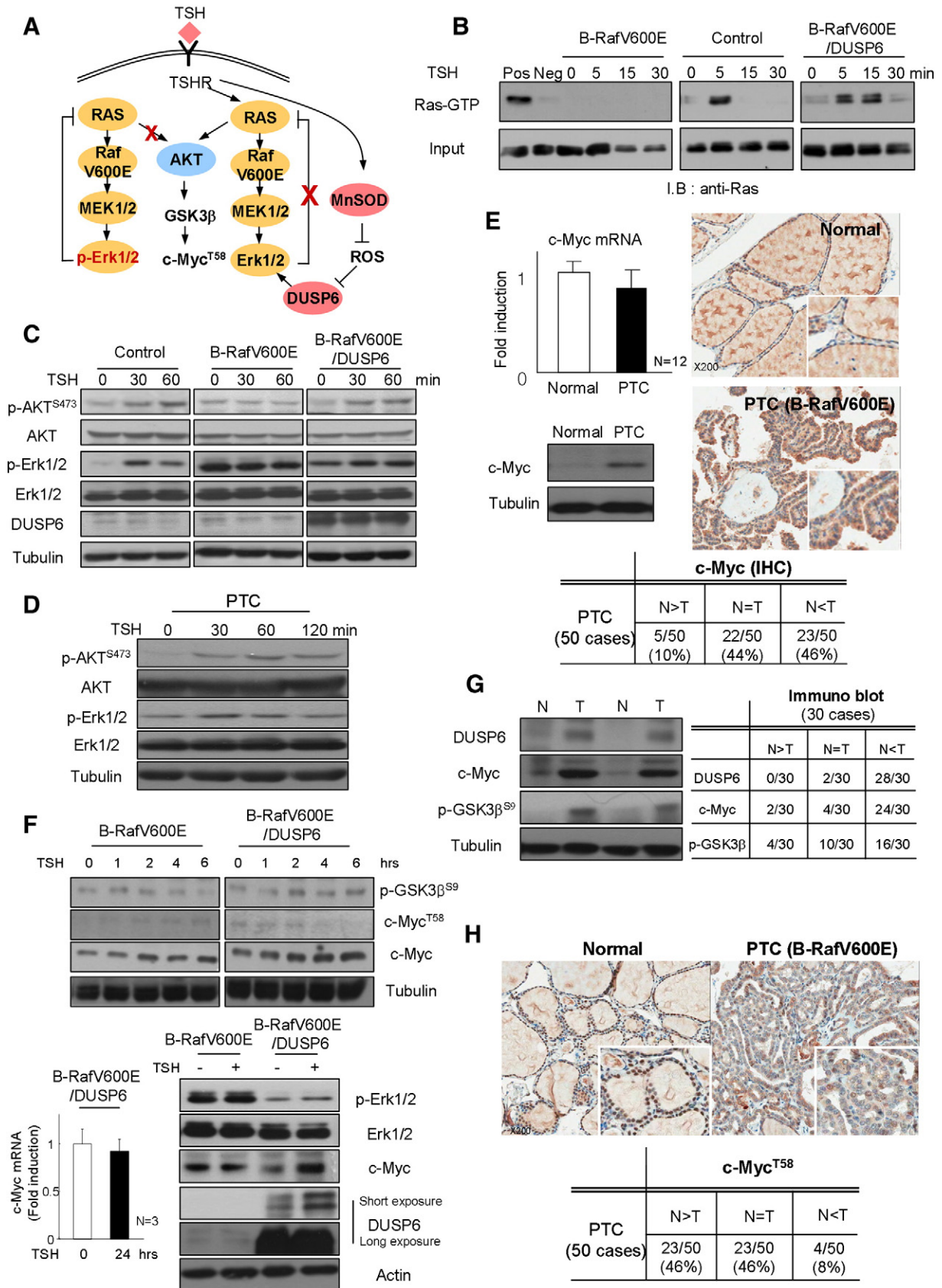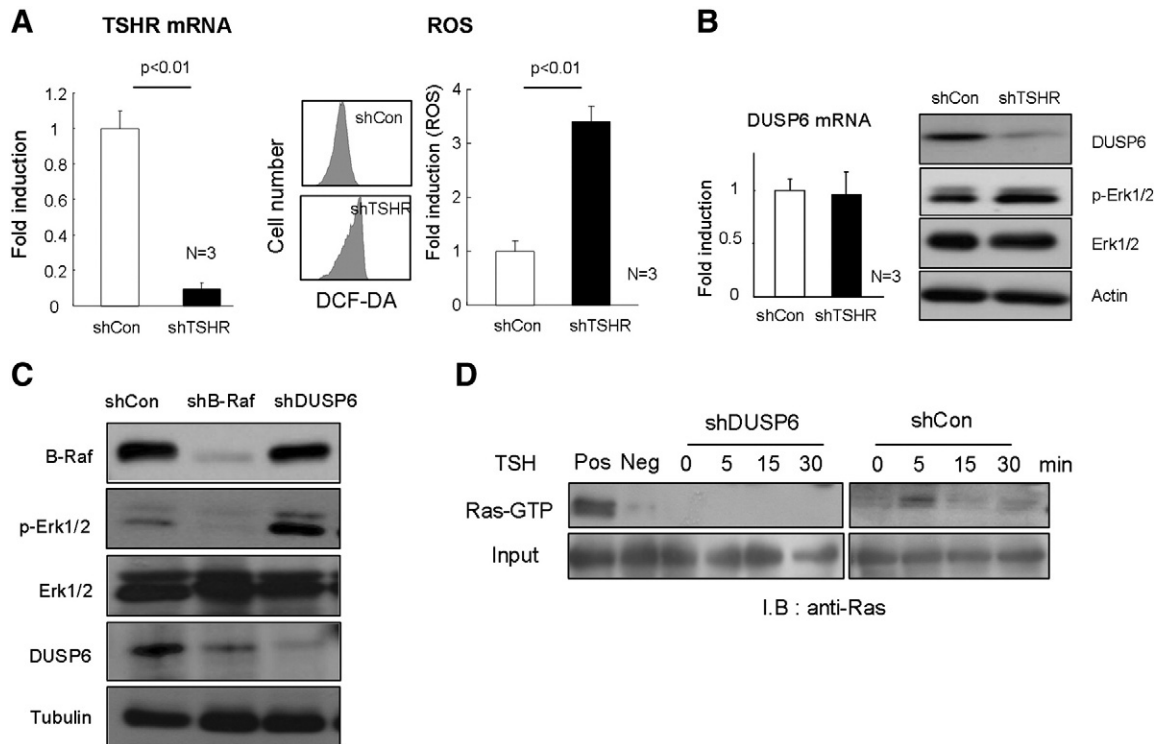
Figure 6. Effect of TSH signaling on SNU790 B-RafV600E PTC cell lines. (A) Knockdown of TSHR increased ROS generation. SNU790 cells were infected with shTSHR lentivirus for 1 week in the presence of TSH (1 mU/ml) and analyzed for TSHR expression by real-time PCR (left panel) and ROS generation (right panel). Bar graph indicates three independent experiments. (B) Knockdown of TSHR decreased DUSP6 protein expression. SNU790 cells were harvested under the same conditions as in A and then analyzed for DUSP6 and p-Erk1/2 expressions by real-time PCR and Western blot. (C) Knockdown of DUSP6 increased p-Erk1/2 expression. SNU790 cells were infected with shB-Raf or shDUSP6, selected with puromycin for 1 week, and then analyzed for p-Erk1/2, B-Raf, and DUSP6 by Western blot analysis. Reactivation of p-Erk1/2 is shown in shDUSP6-expressing cells. (D) Knockdown of DUSP6 did not activate Ras signaling. SNU790 cells were infected with shDUSP6, selected with puromycin for 1 week, and then changed with serum-free media for 24 hours and treated with 1 mU/ml TSH at indicated times and analyzed for GTP-bound Ras by immunoblot.

might be involved in papillary thyroid carcinogenesis. In the present study, therefore, we first focused on factors involving dephosphorylation of Erk1/2 in PTC, since we observed a clear difference of p-Erk1/2 between B-RafV600E–expressing thyrocytes and B-RafV600E–harboring PTC, and recent studies showed that

attenuation or depletion of p-Erk1/2 could prevent the activation of Ras-induced OIS [13,14]. We found that Erk1/2 dephosphorylation was induced by DUSP6 and that DUSP6 was markedly upregulated in human B-RafV600E PTC tissues in agreement with previous studies [16,17,21–23]. Although B-RafV600E induced up-

Figure 5. DUSP6 and TSH reactivated Ras/AKT signaling in B-RafV600E–expressing thyrocytes. (A) Schematic drawing of TSH/TSHR/Ras/AKT or mitogen activated protein kinase pathway. (B) Reactivation of Ras by DUSP6 and TSH. Thyrocytes were infected with control, B-RafV600E, or B-RafV600E/DUSP6 lentivirus and selected with puromycin for 2 weeks. The cells were changed with serum-free media before TSH treatment for 24 hours. The cells were harvested after treatment with TSH (1 mU/ml) at indicated times, and then GTP-bound Ras protein was analyzed by Rho binding protein binding assay. (C) Ras/AKT signaling was reactivated by DUSP6 and TSH. Thyrocytes were infected with control, B-RafV600E, or B-RafV600E/DUSP6 lentivirus and selected with puromycin for 2 weeks. The cells were changed with serum-free media before treatment of TSH for 24 hours. The cells were harvested after treatment with TSH (1 mU/ml) at indicated times and then subjected to Western blot analysis. (D) AKT phosphorylation in B-RafV600E harboring isolated PTC cells. Cancer cells were treated with TSH (1 mU/ml) at indicated times, and p-AKT and p-Erk1/2 expressions were analyzed. (E) c-Myc expression in PTC. c-Myc expression was analyzed by real-time PCR, Western blot analysis, and immunohistochemistry. Fifty cases each of normal and B-RafV600E were analyzed for immunohistochemistry, and the expression level of c-Myc is presented (table). The inset shows higher magnification field. (F) TSH increased c-Myc protein expression. Thyrocytes were treated with 1 mU/ml TSH, and they were then harvested time-dependently (0, 1, 2, 4, and 6 hours) and analyzed for c-Myc, c-Myc^{T58}, and p-glycogen synthase kinase 3β (GSK3β)^{S9} protein expressions by Western blot analysis (upper panel). Thyrocytes were treated with or without TSH (1 mU/ml) for 24 hours and were then harvested and analyzed for p-Erk1/2, c-Myc, and DUSP6. (G) Western blot analysis of DUSP6, c-Myc, and p-GSK3β^{S9}. Thirty cases each of normal and B-RafV600E–harboring PTC region were analyzed, and the expression level is presented (table). (H) Immunohistochemical analysis of c-Myc^{T58} phosphorylation in PTC. Fifty cases each of normal and B-RafV600E were analyzed for immunohistochemistry, and the expression is presented (table). The inset shows higher magnification field. N and T indicate normal and cancer, respectively.
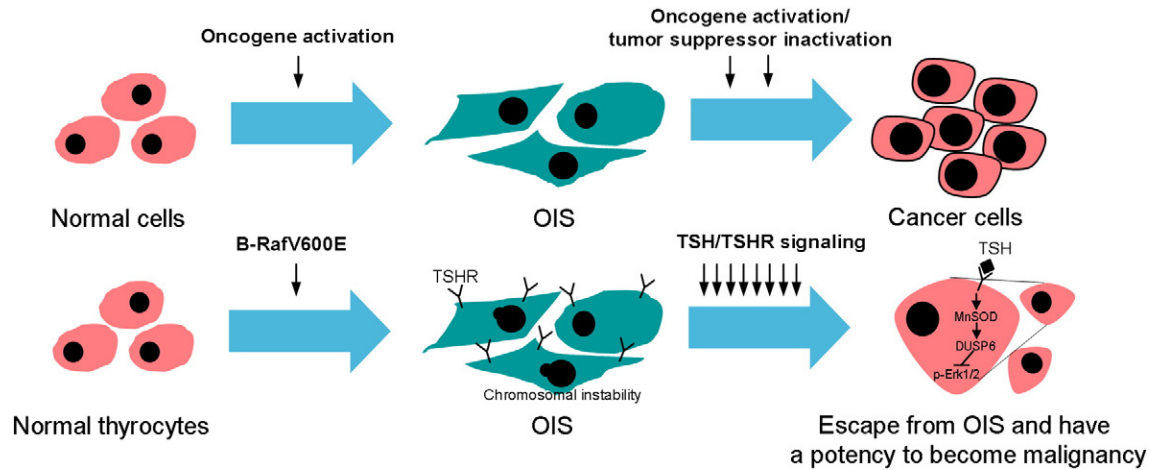
Figure 7. TSH/TSHR signaling together with B-RafV600E induced PTC cooperatively.

regulation of DUSP6 mRNA, OIS itself also increased ROS generation [42]. As a result, DUSP6 could be degraded and inactivated. Under the influence of TSH stimulation, the expression of Mn SOD scavenged ROS sufficiently and was able to reactivate the DUSP6 activity. Degl'Innocenti et al. reported overexpression of DUSP6 in PTC and poorly differentiated carcinoma [22]; however, overexpression of DUSP6 failed to decrease p-Erk1/2 in poorly differentiated carcinoma, which was associated with decreased expression of TSHR [43,44]. This finding also provides evidence supporting that reactivation of DUSP6 depends on TSH signaling.

It has been suggested that TSH stimulation is required to develop PTC in the B-RafV600E transgenic model [27,28]. Several epidemiologic studies also suggest a strong association between TSH levels and risk of malignancy in thyroid, although serum TSH levels in most of the patients with PTC were within normal ranges [45–47], similar to our present result. Previous studies showed that TSHR expression was downregulated in thyroid cancers [43,44]. In the present study, however, we observed increased expression of TSHR in B-RafV600E PTC. In addition, we also found increased expression of TSHR in the B-RafV600E–expressing thyrocytes. We cannot clearly explain these discrepancies between our results and previous observation; nevertheless, we cautiously suggest that these differences might be due to differentiation of tumor cells, because down-regulation of TSHR is observed more frequently in poorly differentiated and undifferentiated carcinomas [43,44]; however, all of the PTCs in the present study were pathologically well-differentiated PTCs. Indeed, increased protein expression of TSHR in PTC has been reported previously [43,48,49]. In addition, several clinical studies reported that serum TSHR mRNA was increased in patients with PTC, but not in patients with benign nodules, and that serum TSHR mRNA could be detected in about 80% of the patients [50,51]. These data indicate that the increase in TSHR mRNA is not uncommon in PTC. Although it has been suggested that B-RafV600E–positive thyroid cancer is associated more frequently with methylation of TSHR gene promotor [52], earlier data on direct correlation between protein expression and mRNA of TSHR are very limited [49]. Therefore, further study is needed to clarify the mechanisms involved in the increase in TSHR in B-RafV600E PTC.

An extensive activation of p-Erk1/2 can inhibit Ras activation [37]. However, Ras activation by TSH in thyrocytes still remains controversial. In Wistar rat thyroid cells, TSH stimulates cell proliferation through cAMP-mediated Ras activation [53]; however, contradictory data have also been reported in dog primary thyrocytes [54], not being fully evaluated in primary human thyrocytes. It is highly possible that TSH can activate Ras through cAMP-mediated pathway in human primary thyrocytes.

Our *in vitro* data showed that Ras/AKT pathway was downregulated in B-RafV600E–expressing cells compared with normal thyrocytes. Overexpression of DUSP6 inhibited p-Erk1/2. Moreover, reactivated Ras had a potential to activate the phosphoinositide 3-kinase pathway. However, our present data indicated that the effects of reactivation of DUSP6 and TSH were limited to the inhibition of OIS, and further transformation signaling seems to be required to develop PTC. At that point, therefore, we focused on c-Myc expression in PTC. Although c-Myc mRNA level was not changed, protein level seemed to be controlled by a posttranslational event. These results led us to suggest the possibility that reactivation of Ras/AKT signaling by TSH and DUSP6 involves GSK3β phosphorylation, which in turn induces c-Myc stabilization and represents as an overexpression of c-Myc.

At this point, we asked a question of what is the role of B-RafV600E mutation in papillary thyroid carcinogenesis. First, B-RafV600E is associated with TSHR overexpression in early stage of thyroid carcinogenesis. Higher expression of TSHR is a unique phenotype of B-RafV600E PTC. We also analyzed the expression of TSHR in the B-Raf wild-type PTC and found that the immunoexpression of TSHR was not as strong as that of B-RafV600E–harboring PTCs (Figure S7). The present results suggest that TSH/TSHR signaling helps cells escape from OIS through downregulation of ROS and activation of DUSP6. Second, B-RafV600E induces chromosomal instability. We found that the cell cycle was blocked at the S phase (data not shown) and centrosome number was markedly increased by B-RafV600E, resulting in aneuploid formation (Figure S8). We did not include it in the Results section, because these phenotypes have already been observed by Liu et al. [55] and Mitsutake et al. [56]; Liu et al. suggested that Msp1 phosphorylated by B-RafV600E contributes to chromosome instability in melanoma [55]. Therefore, our experimental results together with the above-mentioned studies suggest that B-RafV600E could initiate cancer formation by regulation of chromosome stability.

Most cancers are developed by activation of several kinds of oncogene or combined tumor suppressor gene inactivation; "two or multiple hits" are required for cancer formation. However, B-RafV600E expression is enough to induce PTC [27], suggesting that "one hit; B-RafV600E" is enough to develop a cancer in the thyroid. Since senescence is a good barrier to develop a cancer, it is highly possible that B-RafV600E mutation can develop a cancer in the thyroid if a program to overcome senescence co-exists. Therefore, our present data strongly suggest that OIS was overcome by hormone stimulation in the absence of additional oncogene or tumor suppressor gene dysregulation. We could not perform a cancer formation assay such as nude mouse injection, because one-oncogene activation and hormonal stimulation are not strong inducers for cancer development. We also tried double lentivirus delivery into thyrocytes, including B-RafV600E/c-Myc with TSH. Although we found some of these cells with morphologic changes that were consistent with the transformation (Figure S9), we could not carry out further observation because of massive cell death. Consequently, we could not fully explain the exact mechanism involved in papillary thyroid carcinogenesis. Nevertheless, we cautiously suggest that B-RafV600E mutation and TSH signaling cooperatively induced PTC (Figure 7).

Conclusion

We herein showed that B-RafV600E and TSH cooperatively play critical roles in papillary thyroid carcinogenesis and suggest that inhibition of B-RafV600E together with TSHR can inhibit tumor progression more efficiently in B-RafV600E–harboring PTC.

Supplementary data to this article can be found online at http://dx.doi.org/10.1016/j.neo.2014.10.005.

Acknowledgment

References

[1] Xing M (2013). Molecular pathogenesis and mechanisms of thyroid cancer. *Nat Rev Cancer* **13**, 184–199.

[2] Xing M (2007). BRAF mutation in papillary thyroid cancer: pathogenic role, molecular bases, and clinical implications. *Endocr Rev* **28**, 742–762.

[3] Kimura ET, Nikiforova MN, Zhu Z, Knauf JA, Nikiforov YE, and Fagin JA (2003). High prevalence of *BRAF* mutations in thyroid cancer: genetic evidence for constitutive activation of the RET/PTC-RAS-BRAF signaling pathway in papillary thyroid carcinoma. *Cancer Res* **63**, 1454–1457.

[4] Singer G, Oldt III R, Cohen Y, Wang BG, Sidransky D, Kurman RJ, and Shih Ie M (2003). Mutations in BRAF and KRAS characterize the development of low-grade ovarian serous carcinoma. *J Natl Cancer Inst* **95**, 484–486.

[5] Pollock PM, Harper UL, Hansen KS, Yudt LM, Stark M, Robbins CM, Moses TY, Hostetter G, Wagner U, and Kakareka J, et al (2003). High frequency of BRAF mutations in nevi. *Nat Genet* **33**, 19–20.

[6] Yuen ST, Davies H, Chan TL, Ho JW, Bignell GR, Cox C, Stephens P, Edkins S, Tsui WW, and Chan AS, et al (2002). Similarity of the phenotypic patterns associated with BRAF and KRAS mutations in colorectal neoplasia. *Cancer Res* **62**, 6451–6455.

[7] Davies H, Bignell GR, Cox C, Stephens P, Edkins S, Clegg S, Teague J, Woffendin H, Garnett MJ, and Bottomley W, et al (2002). Mutations of the BRAF gene in human cancer. *Nature* **417**, 949–954.

[8] Nikiforova MN, Kimura ET, Gandhi M, Biddinger PW, Knauf JA, Basolo F, Zhu Z, Giannini R, Salvatore G, and Fusco A, et al (2003). BRAF mutations in thyroid tumors are restricted to papillary carcinomas and anaplastic or poorly differentiated carcinomas arising from papillary carcinomas. *J Clin Endocrinol Metab* **88**, 5399–5404.

[9] Vizioli MG, Possik PA, Tarantino E, Meissl K, Borrello MG, Miranda C, Anania MC, Pagliardini S, Seregni E, and Pierotti MA, et al (2011). Evidence of oncogene-induced senescence in thyroid carcinogenesis. *Endocr Relat Cancer* **18**, 743–757.

[10] Wajapeyee N, Serra RW, Zhu X, Mahalingam M, and Green MR (2008). Oncogenic BRAF induces senescence and apoptosis through pathways mediated by the secreted protein IGFBP7. *Cell* **132**, 363–374.

[11] Michaloglou C, Vredeveld LC, Soengas MS, Denoyelle C, Kuilman T, van der Horst CM, Majoor DM, Shay JW, Mooi WJ, and Peeper DS (2005). BRAF^{E600}-associated senescence-like cell cycle arrest of human naevi. *Nature* **436**, 720–724.

[12] Serrano M, Lin AW, McCurrach ME, Beach D, and Lowe SW (1997). Oncogenic ras provokes premature cell senescence associated with accumulation of p53 and p16INK4a. *Cell* **88**, 593–602.

[13] Deschenes-Simard X, Gaumont-Leclerc MF, Bourdeau V, Lessard F, Moiseeva O, Forest V, Igelmann S, Mallette FA, Saba-El-Leil MK, and Meloche S, et al (2013). Tumor suppressor activity of the ERK/MAPK pathway by promoting selective protein degradation. *Genes Dev* **27**, 900–915.

[14] Shin J, Yang J, Lee JC, and Baek KH (2013). Depletion of ERK2 but not ERK1 abrogates oncogenic Ras-induced senescence. *Cell Signal* **25**, 2540–2547.

[15] Mooi WJ and Peeper DS (2006). Oncogene-induced cell senescence—halting on the road to cancer. *N Engl J Med* **355**, 1037–1046.

[16] Kim SW, Kim HK, Lee JI, Jang HW, Choe JH, Kim JH, Kim JS, Hur KY, Kim JH, and Chung JH (2013). ERK phosphorylation is not increased in papillary thyroid carcinomas with BRAF(V600E) mutation compared to that of corresponding normal thyroid tissues. *Endocr Res* **38**, 89–97.

[17] Zuo H, Nakamura Y, Yasuoka H, Zhang P, Nakamura M, Mori I, Miyauchi A, and Kakudo K (2007). Lack of association between BRAF V600E mutation and mitogen-activated protein kinase activation in papillary thyroid carcinoma. *Pathol Int* **57**, 12–20.

[18] Zhang Z, Kobayashi S, Borczuk AC, Leidner RS, Laframboise T, Levine AD, and Halmos B (2010). Dual specificity phosphatase 6 (DUSP6) is an ETS-regulated negative feedback mediator of oncogenic ERK signaling in lung cancer cells. *Carcinogenesis* **31**, 577–586.

[19] Ekerot M, Stavridis MP, Delavaine L, Mitchell MP, Staples C, Owens DM, Keenan ID, Dickinson RJ, Storey KG, and Keyse SM (2008). Negative-feedback regulation of FGF signalling by DUSP6/MKP-3 is driven by ERK1/2 and mediated by Ets factor binding to a conserved site within the DUSP6/MKP-3 gene promoter. *Biochem J* **412**, 287–298.

[20] Ouyang B, Knauf JA, Smith EP, Zhang L, Ramsey T, Yusuff N, Batt D, and Fagin JA (2006). Inhibitors of Raf kinase activity block growth of thyroid cancer cells with RET/PTC or BRAF mutations in vitro and in vivo. *Clin Cancer Res* **12**, 1785–1793.

[21] Lee EK, Chung KW, Yang SK, Park MJ, Min HS, Kim SW, and Kang HS (2013). DNA methylation of MAPK signal-inhibiting genes in papillary thyroid carcinoma. *Anticancer Res* **33**, 4833–4839.

[22] Degl'Innocenti D, Romeo P, Tarantino E, Sensi M, Cassinelli G, Catalano V, Lanzi C, Perrone F, Pilotti S, and Seregni E, et al (2013). DUSP6/MKP3 is overexpressed in papillary and poorly differentiated thyroid carcinoma and contributes to neoplastic properties of thyroid cancer cells. *Endocr Relat Cancer* **20**, 23–37.

[23] Lee JU, Huang S, Lee MH, Lee SE, Ryu MJ, Kim SJ, Kim YK, Kim SY, Joung KH, and Kim JM, et al (2012). Dual specificity phosphatase 6 as a predictor of invasiveness in papillary thyroid cancer. *Eur J Endocrinol* **167**, 93–101.

[24] Dhomen N, Reis-Filho JS, da Rocha Dias S, Hayward R, Savage K, Delmas V, Larue L, Pritchard C, and Marais R (2009). Oncogenic Braf induces melanocyte senescence and melanoma in mice. *Cancer Cell* **15**, 294–303.

[25] Dankort D, Curley DP, Cartlidge RA, Nelson B, Karnezis AN, Damsky Jr WE, You MJ, DePinho RA, McMahon M, and Bosenberg M (2009). Braf(V600E) cooperates with Pten loss to induce metastatic melanoma. *Nat Genet* **41**, 544–552.

[26] Dankort D, Filenova E, Collado M, Serrano M, Jones K, and McMahon M (2007). A new mouse model to explore the initiation, progression, and therapy of BRAFV600E-induced lung tumors. *Genes Dev* **21**, 379–384.

[27] Franco AT, Malaguarnera R, Refetoff S, Liao XH, Lundsmith E, Kimura S, Pritchard C, Marais R, Davies TF, and Weinstein LS, et al (2011). Thyrotrophin receptor signaling dependence of Braf-induced thyroid tumor initiation in mice. *Proc Natl Acad Sci U S A* **108**, 1615–1620.

[28] Knauf JA, Ma X, Smith EP, Zhang L, Mitsutake N, Liao XH, Refetoff S, Nikiforov YE, and Fagin JA (2005). Targeted expression of BRAFV600E in thyroid cells of transgenic mice results in papillary thyroid cancers that undergo dedifferentiation. *Cancer Res* **65**, 4238–4245.

[29] Shimamura M, Nakahara M, Orim F, Kurashige T, Mitsutake N, Nakashima M, Kondo S, Yamada M, Taguchi R, and Kimura S, et al (2013). Postnatal

expression of BRAFV600E does not induce thyroid cancer in mouse models of thyroid papillary carcinoma. *Endocrinology* **154**, 4423–4430.

[30] Kim YH, Choi MH, Kim JH, Lim IK, and Park TJ (2013). C-terminus-deleted FoxM1 is expressed in cancer cell lines and induces chromosome instability. *Carcinogenesis* **34**, 1907–1917.

[31] Chung KW, Yang SK, Lee GK, Kim EY, Kwon S, Lee SH, Park do J, Lee HS, Cho BY, and Lee ES, et al (2006). Detection of BRAFV600E mutation on fine needle aspiration specimens of thyroid nodule refines cyto-pathology diagnosis, especially in BRAF600E mutation-prevalent area. *Clin Endocrinol (Oxf)* **65**, 660–666.

[32] Capper D, Preusser M, Habel A, Sahm F, Ackermann U, Schindler G, Pusch S, Mechtersheimer G, Zentgraf H, and von Deimling A (2011). Assessment of BRAF V600E mutation status by immunohistochemistry with a mutation-specific monoclonal antibody. *Acta Neuropathol* **122**, 11–19.

[33] Chen Z, Trotman LC, Shaffer D, Lin HK, Dotan ZA, Niki M, Koutcher JA, Scher HI, Ludwig T, and Gerald W, et al (2005). Crucial role of p53-dependent cellular senescence in suppression of Pten-deficient tumorigenesis. *Nature* **436**, 725–730.

[34] Collado M, Gil J, Efeyan A, Guerra C, Schuhmacher AJ, Barradas M, Benguria A, Zaballos A, Flores JM, and Barbacid M, et al (2005). Tumour biology: senescence in premalignant tumours. *Nature* **436**, 642.

[35] Chan DW, Liu VW, Tsao GS, Yao KM, Furukawa T, Chan KK, and Ngan HY (2008). Loss of MKP3 mediated by oxidative stress enhances tumorigenicity and chemoresistance of ovarian cancer cells. *Carcinogenesis* **29**, 1742–1750.

[36] Kim HS, Song MC, Kwak IH, Park TJ, and Lim IK (2003). Constitutive induction of p-Erk1/2 accompanied by reduced activities of protein phosphatases 1 and 2A and MKP3 due to reactive oxygen species during cellular senescence. *J Biol Chem* **278**, 37497–37510.

[37] Pratilas CA, Taylor BS, Ye Q, Viale A, Sander C, Solit DB, and Rosen N (2009). (V600E)BRAF is associated with disabled feedback inhibition of RAF-MEK signaling and elevated transcriptional output of the pathway. *Proc Natl Acad Sci U S A* **106**, 4519–4524.

[38] Sears R, Nuckolls F, Haura E, Taya Y, Tamai K, and Nevins JR (2000). Multiple Ras-dependent phosphorylation pathways regulate Myc protein stability. *Genes Dev* **14**, 2501–2514.

[39] Zhang X, Farrell AS, Daniel CJ, Arnold H, Scanlan C, Laraway BJ, Janghorban M, Lum L, Chen D, and Troxell M, et al (2012). Mechanistic insight into Myc stabilization in breast cancer involving aberrant Axin1 expression. *Proc Natl Acad Sci U S A* **109**, 2790–2795.

[40] Tuveson DA, Shaw AT, Willis NA, Silver DP, Jackson EL, Chang S, Mercer KL, Grochow R, Hock H, and Crowley D, et al (2004). Endogenous oncogenic K-ras (G12D) stimulates proliferation and widespread neoplastic and developmental defects. *Cancer Cell* **5**, 375–387.

[41] Guerra C, Mijimolle N, Dhawahir A, Dubus P, Barradas M, Serrano M, Campuzano V, and Barbacid M (2003). Tumor induction by an endogenous K-ras oncogene is highly dependent on cellular context. *Cancer Cell* **4**, 111–120.

[42] Lee AC, Fenster BE, Ito H, Takeda K, Bae NS, Hirai T, Yu ZX, Ferrans VJ, Howard BH, and Finkel T (1999). Ras proteins induce senescence by altering the intracellular levels of reactive oxygen species. *J Biol Chem* **274**, 7936–7940.

[43] Matsumoto H, Sakamoto A, Fujiwara M, Yano Y, Shishido-Hara Y, Fujioka Y, and Kamma H (2008). Decreased expression of the thyroid-stimulating hormone receptor in poorly-differentiated carcinoma of the thyroid. *Oncol Rep* **19**, 1405–1411.

[44] Sheils OM and Sweeney EC (1999). TSH receptor status of thyroid neoplasms—TaqMan RT-PCR analysis of archival material. *J Pathol* **188**, 87–92.

[45] Boelaert K (2009). The association between serum TSH concentration and thyroid cancer. *Endocr Relat Cancer* **16**, 1065–1072.

[46] Haymart MR, Repplinger DJ, Leverson GE, Elson DF, Sippel RS, Jaume JC, and Chen H (2008). Higher serum thyroid stimulating hormone level in thyroid nodule patients is associated with greater risks of differentiated thyroid cancer and advanced tumor stage. *J Clin Endocrinol Metab* **93**, 809–814.

[47] Boelaert K, Horacek J, Holder RL, Watkinson JC, Sheppard MC, and Franklyn JA (2006). Serum thyrotropin concentration as a novel predictor of malignancy in thyroid nodules investigated by fine-needle aspiration. *J Clin Endocrinol Metab* **91**, 4295–4301.

[48] So YK, Son YI, Baek CH, Jeong HS, Chung MK, and Ko YH (2012). Expression of sodium-iodide symporter and TSH receptor in subclinical metastatic lymph nodes of papillary thyroid microcarcinoma. *Ann Surg Oncol* **19**, 990–995.

[49] Wang ZF, Liu QJ, Liao SQ, Yang R, Ge T, He X, Tian CP, and Liu W (2011). Expression and correlation of sodium/iodide symporter and thyroid stimulating hormone receptor in human thyroid carcinoma. *Tumori* **97**, 540–546.

[50] Milas M, Shin J, Gupta M, Novosel T, Nasr C, Brainard J, Mitchell J, Berber E, and Siperstein A (2010). Circulating thyrotropin receptor mRNA as a novel marker of thyroid cancer: clinical applications learned from 1758 samples. *Ann Surg* **252**, 643–651.

[51] Qiu J, Zhang Y, Guo X, Zeng F, Zhao C, Qiu X, and Wu X (2010). Quantitation of thyroid-stimulating hormone receptor mRNA with real-time PCR for early diagnosis of papillary thyroid microcarcinoma. *Neoplasma* **57**, 360–364.

[52] Khan MS, Pandith AA, Masoodi SR, Wani KA, Ul Hussain M, and Mudassar S (2014). Epigenetic silencing of TSHR gene in thyroid cancer patients in relation to their BRAF V600E mutation status. *Endocrine* **47**, 449–455.

[53] Tsygankova OM, Kupperman E, Wen W, and Meinkoth JL (2000). Cyclic AMP activates Ras. *Oncogene* **19**, 3609–3615.

[54] Van Keymeulen A, Roger PP, Dumont JE, and Dremier S (2000). TSH and cAMP do not signal mitogenesis through Ras activation. *Biochem Biophys Res Commun* **273**, 154–158.

[55] Liu J, Cheng X, Zhang Y, Li S, Cui H, Zhang L, Shi R, Zhao Z, He C, and Wang C, et al (2013). Phosphorylation of Mps1 by BRAFV600E prevents Mps1 degradation and contributes to chromosome instability in melanoma. *Oncogene* **32**, 713–723.

[56] Mitsutake N, Knauf JA, Mitsutake S, Mesa Jr C, Zhang L, and Fagin JA (2005). Conditional BRAFV600E expression induces DNA synthesis, apoptosis, dedifferentiation, and chromosomal instability in thyroid PCCL3 cells. *Cancer Res* **65**, 2465–2473.